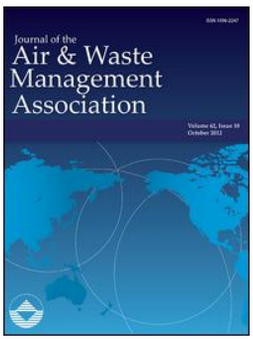

Journal of the Air & Waste Management Association

ISSN: 1096-2247 (Print) 2162-2906 (Online) Journal homepage: https://www.tandfonline.com/loi/uawm20

Innovative Approach for Estimating Fugitive Gaseous Fluxes Using Computed Tomography and Remote Optical Sensing Techniques

Ram A. Hashmonay & Michael G. Yost

To cite this article: Ram A. Hashmonay & Michael G. Yost (1999) Innovative Approach for Estimating Fugitive Gaseous Fluxes Using Computed Tomography and Remote Optical Sensing Techniques, Journal of the Air & Waste Management Association, 49:8, 966-972, DOI: 10.1080/10473289.1999.10463862

To link to this article: https://doi.org/10.1080/10473289.1999.10463862

TECHNICAL PAPER

ISSN 1047-3289 *J. Air & Waste Manage. Assoc.* **49**:966-972

Innovative Approach for Estimating Fugitive Gaseous Fluxes Using Computed Tomography and Remote Optical Sensing Techniques

Ram A. Hashmonay and Michael G. Yost
Department of Environmental Health, University of Washington, Seattle, Washington

ABSTRACT

This paper presents a new approach to quantify emissions from fugitive gaseous air pollution sources. The authors combine Computed Tomography (CT) with Path-Integrated Optical Remote Sensing (PI-ORS) concentration data in a new field beam geometry. Path-integrated concentrations are sampled in a vertical plane downwind from the source along several radial beam paths. An innovative CT technique, which applies the Smooth Basis Function Minimization method to the beam data in conjunction with measured wind data, is used to estimate the total flux from the fugitive source. The authors conducted a synthetic data study to evaluate the proposed methodology under different meteorological conditions, beam geometry configurations, and simulated measurement errors. The measurement errors were simulated based on data collected with an Open-Path Fourier Transform Infra-Red system. This approach was found to be robust for the simulated errors and for a wide range of fluctuating wind directions. In the very sparse beam geometry examined (eight beam paths), successful emission rates were retrieved over a 70° range of wind directions under extremely large measurement error conditions.

IMPLICATIONS

The suggested technology may provide robust and real time estimates of emission rates and near field dispersion parameters for especially near ground level fugitive sources. This system could either survey sources to improve the source's emission profile or be applied as an alarm for the source's departure from normal working conditions. In this case, the beam plane should be located between the source and the concerned neighboring communities to alert to a potential emergency. The estimated flux and dispersion parameters' atmospheric stability condition indicators could be used in a dispersion model to calculate in near real time the downwind field of concentrations.

INTRODUCTION

This paper applies Path-Integrated Optical Remote Sensing (PI-ORS) and innovative Computed Tomography (CT) techniques to determine fluxes from fugitive gaseous air pollution sources. The described methodology is designed to provide an applicable PI-ORS monitoring approach in sparse beam geometries for estimating the total emission rate directly from the measured concentration and wind data, without employing any dispersion model dependent assumptions. An overall aim of this study is to provide measures of the initial near field dispersion parameters based on CT-reconstructed maps along with improved estimates of total emission rate. These important parameters provide the essential data needed for a dispersion model to produce reliable exposure estimates for downwind neighboring communities.

Several methods have been developed and applied[1–9] in the past to estimate emission rates from fugitive sources, such as landfills,[3] coal mines,[5,6] or water treatment plants,[7,8] using PI-ORS technologies. All previous methodologies combine downwind Path-Integrated Concentration (PIC) data, wind measurements, and plume dispersion modeling assumptions to retrieve the total emission rate. The ideal approach for measuring the flux from an upwind emission source would be to directly measure the integrated concentration across the entire cross-wind vertical plane located downwind from the emission source. Multiplying by the *averaged* wind speed (weighted average by heights if several wind monitors are mounted in different elevations) component in the normal direction to the vertical plane provides the flux flowing through this plane and, therefore, the upwind source's emission rate. In most situations, it is impractical to directly measure the plane-integrated concentration using PI-ORS methods due to the complex beam configuration needed to cover all of the relevant plane.[2,7,8] Alternatively, another technique, such as Differential Absorption LIDAR (DIAL), could be applied to directly measure a spatially resolved map of the contaminant concentrations.[10] Integrating the concentration over

the whole map provides the required plane-integrated concentration. Cost, a limited number of potentially detectable target contaminants, high detection limits, and calibration difficulties so far have prevented the wide application of DIAL technology. In recent methods[3,4] the PI-ORS instrument is scanned diagonally from a fixed ground level location to retroreflectors at different heights to partially cover the vertical plane. Dispersion modeling was applied to interpolate and extrapolate the measured data and generate the plane-integrated concentrations. However, our recent validation study[9] for fugitive source apportionment of emission rates suggests that relying on dispersion models in near field conditions may produce inconsistent estimates of the total emission rate. Our results suggest that scanning solely on the ground level as suggested by earlier methods[1,5,6] is not sufficient for estimation of the flux flowing through a vertical plane, even for a ground level source. Furthermore, extrapolation of slanted PIC values to recover the whole plane-integrated concentration based on a dispersion-modeled vertical profile could yield erroneous estimation of the derived total emission rates.

Recently the authors' CT efforts have focused on developing an algorithm that will allow reconstruction of a concentration field in a plane, based on non-overlapping PIC data scanned in radial alternating path lengths.[11] The authors and others[11,12] have shown that the Smooth Basis Functions Minimization (SBFM) approach[13] can provide the desired field of concentration with a relatively sparse beam geometry. The authors suggest applying this innovative SBFM approach to reconstruct the smoothed field of concentration in the downwind vertical plane. This will allow the plane-integrated concentration to be calculated and, thus, the emission flux. With this SBFM approach, the plume dimensions can be *directly* reconstructed based on the acquired PIC data, as opposed to previous methods that are dispersion model–dependent. Reconstructions based on other more "classical" CT algorithms using intersecting beams[13] have much more complex beam geometries and may not provide the plane-integrated concentration, because they are limited to the area where the beams overlap. Applying a sparse beam geometry with the SBFM algorithm to the vertical plane should allow more accurate calculation of the desired plane-integrated concentration.

Methodology

The following section describes the authors' general approach to this estimation problem and also discusses some future developments of the suggested methodology. The proposed methodology uses a two-dimensional SBFM-CT technique applied to PI-ORS data to reconstruct the cross-wind concentration map in a vertical plane. The plane-integrated concentration from this reconstruction, along with the averaged wind data, provide an estimate of the total flux from the emission source. The key to this methodology is a rather simple and sparse PI-ORS beam geometry that allows reconstruction of smoothed concentration maps in a downwind vertical plane. An example showing the suggested radial nonoverlapping beam geometry and an upwind point source is illustrated in Figure 1. This beam geometry includes eight beam paths approximately in the cross-wind vertical plane. Four beam-paths are on the ground level with different path-lengths and the other four are elevated in two locations along the cross-wind direction. We suggest scanning the PI-ORS instrument among the beam paths for at least 20 min to allow a buildup of an approximate Gaussian plume. Wind speed and direction data would be collected and averaged over the same time interval.

To develop a reliable time-averaged plume profile, it is desirable to get as many repeats as possible at each beam path. Therefore, the sampling time at each retroreflector should be as short as practical limits allow. For example, when applying Open Path Fourier Transform Infra-Red (OP-FTIR) instruments, this sampling time for each beam path is limited by spectral resolution and the desired detection limit. Typically a 10-sec averaging time, resulting in high detection limits for most compounds, is a practical limit for OP-FTIR. This relatively short time will allow the PI-ORS device to aim back about 10 times to the same retroreflector over a 20-min interval, allowing about five seconds for moving between retroreflectors. Then the PIC data should be time-averaged for each beam path prior to the application of the CT reconstruction method.

The authors used the SBFM reconstruction approach with a two-dimensional smooth basis function (bi-variate Gaussian) to estimate the total emission rate. In the SBFM

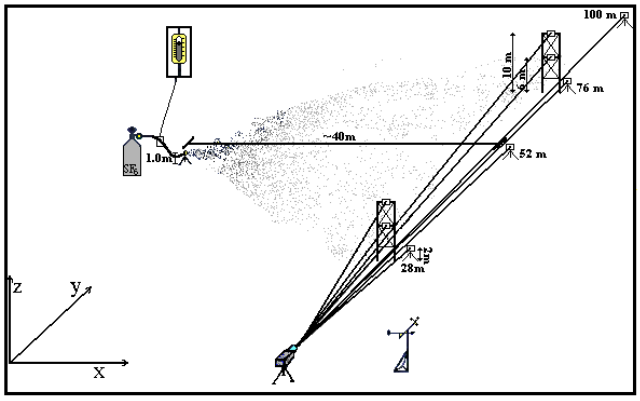

Figure 1. Simulated field configuration and Optical Remote Sensing (ORS) beam geometry. The beam geometry is in a vertical plane 40 meters downwind from a controlled emission point source. The beam geometry consists of eight beam paths, four scanning the ORS device to ground-level (two meters height) retroreflectors and four slanted beam paths scanning the ORS device to elevated (6 and 10 meters height) retroreflectors mounted on two towers.

approach, a known smooth basis function or a superposition of such functions with unknown parameters are assumed to describe the distribution of concentrations. Instead of trying to find the concentration value in each pixel, the search is for the unknown parameters of the basis functions. The latter characteristic of the SBFM approach led the authors to realize that radial scanning of a nonoverlapping beam geometry might be sufficient to retrieve the air pollutant concentration field. In our earlier studies,[14] the authors used several bi-variate Gaussian functions as the smooth basis functions. Since the authors' interest is in the plane-integrated concentration and not the exact map of concentrations in the plane, we suggest fitting only one smooth basis function (one bi-variate Gaussian) to reconstruct the smooth map. However, it is important to emphasize that the authors do not assume in this methodology that the true distribution of concentration in the vertical plane is a bi-variate Gaussian. The authors show in this study that one can fit a single bi-variate Gaussian to many kinds of skewed distributions and still retrieve a reasonably good estimate of the plane-integrated concentration. The authors also examined the fit of a single bi-variate Gaussian to a multiple mode distribution and found the reconstructed plane-integrated concentration to conserve fairly well the test plane-integrated concentration.

In each iterative step of the SBFM-CT search procedure to find the distribution in parameters, the measured PIC values are compared with assumed PIC values calculated from the new set of parameters. To compute the assumed PIC values, one has to integrate the basis function along the beam paths. Therefore, in the radial beam geometry it is more convenient to express a bi-variate Gaussian distribution in polar coordinates, $G(r,\theta)$:

$$G(r,\theta) = \frac{A}{2\pi\sigma_y\sigma_z\sqrt{1-\rho_{12}^2}} \exp\left\{-\frac{1}{2(1-\rho_{12}^2)}\right.$$

$$\left.\left[\frac{(r\cos\theta - m_y)^2}{\sigma_y^2} - \frac{2\rho_{12}(r\cos\theta - m_y)(r\sin\theta - m_z)}{\sigma_y\sigma_z} + \frac{(r\sin\theta - m_z)^2}{\sigma_z^2}\right]\right\} \quad (1)$$

where r is the distance from the PI-ORS instrument and θ is the angle created between the beam and the horizontal plane intersecting the PI-ORS instrument location. As shown in eq 1, each bi-variate Gaussian has six unknown independent parameters: (1) A is a normalizing coefficient that adjusts for the volume under the bi-variate surface; (2) ρ_{12} is a correlation coefficient that defines the direction of the distribution-independent variations in relation to the Cartesian directions y and z (ρ_{12}=0 means that the distribution variations overlap the Cartesian coordinates); (3) m_y and z_z are peak locations in Cartesian coordinates; and (4) σ_y and σ_z are standard deviations in Cartesian coordinates.

To fit the unknown parameters of the smooth basis functions to the PIC data, one has to define an error function for minimization. As opposed to the authors' earlier studies,[14] which minimized the Root Mean Squares (RMS) error function, we chose to minimize the Sum of Squared Errors (SSE) function, which provides the least squares fit between the measured PIC values and the calculated PIC values from integration through the assumed smooth basis function. The SSE function is defined in our study as follows:

$$SSE(A, \rho_{12}, m_y, m_z, \sigma_y, \sigma_z) = \sum_i \left[PIC_i - \int_0^{r_i} G(r,\theta_i)dr\right]^2 \quad (2)$$

where *PIC* represents the measured PIC values, and the index *i* is for the different beams. The SSE function is minimized using an iterative minimization procedure, such as the Simplex method, or Simulated Annealing,[15] to solve for the unknown parameters.

As mentioned earlier, the authors' interest is in the plane-integrated concentration, and therefore, we fit one bi-variate Gaussian surface to match the volume under the underlying true concentration distribution surface. This volume is highly conserved in the fitting procedure, which emphasizes agreement over many path integrals. Six independent beam paths are sufficient to determine one bi-variate Gaussian, which has six independent unknown parameters.

Some reasonable assumptions also may be made when applying the SBFM-CT method to this problem, such as setting the correlation factor parameter equal to zero. This assumption means that the reconstructed bi-variate Gaussian is limited to changes in the vertical and cross-wind directions only. One also can fix the peak location in the vertical direction to the ground level when ground-level emissions are known to exist. The same could be done to the peak location in the cross-wind direction, using *a priori* knowledge on wind direction and source location. However in our methodology, in contrast to earlier methodologies, there is no need to apply a priori information on the source location and configuration, and therefore, the authors chose not to use this assumption.

In most of the previous methodologies, OP-FTIR instruments were used as the PI-ORS device, mainly due to its simultaneous chemical analysis capability. However, when only a few species are of interest, it might be more efficient to employ other laser-based PI-ORS technologies like Tunable Diode Laser (TDL) or Path Integrated DIAL, which have longer ranges and faster scanning capabilities.

Computational Study

The objective of the synthetic study was to evaluate the feasibility and robustness of the suggested beam geometry and CT algorithm for total emission rate estimation under realistic changing meteorological and noise conditions. We used a Gaussian dispersion model (PAL)[16] only for generating the time-averaged concentration test maps in a vertical plane 40 meters downwind from a ground-level point source (one-meter height). Concentration values were calculated for every 4×4 meters-square elementary unit in a vertical domain size of 100×24 meters. The authors calculated test maps every five degrees of wind direction up to $\pm$ 55 degrees from the normal situation in Pasquill's stability[17] category B; 23 test maps were created overall.

The PAL dispersion model should be mass-conserving, so the plane-integrated concentrations of all calculated test maps were examined to check for agreement with the input emission rate of 1 g/sec. Since the input wind speed was 1 m/sec, the reconstructed emission rate was calculated by numerical integration over the entire test map followed by multiplication of the latter by the cosine of the wind shift angle, when the vertical plane was not perpendicular to the wind direction. All the test map integration calculations agreed within 1% compared to the input data.

The test map of the normal cross-wind situation is very close to a symmetric bi-variate Gaussian distribution. However, all the other maps are nonsymmetrical and the larger the wind shift angle, the more skewed is the distribution (see Figure 2).

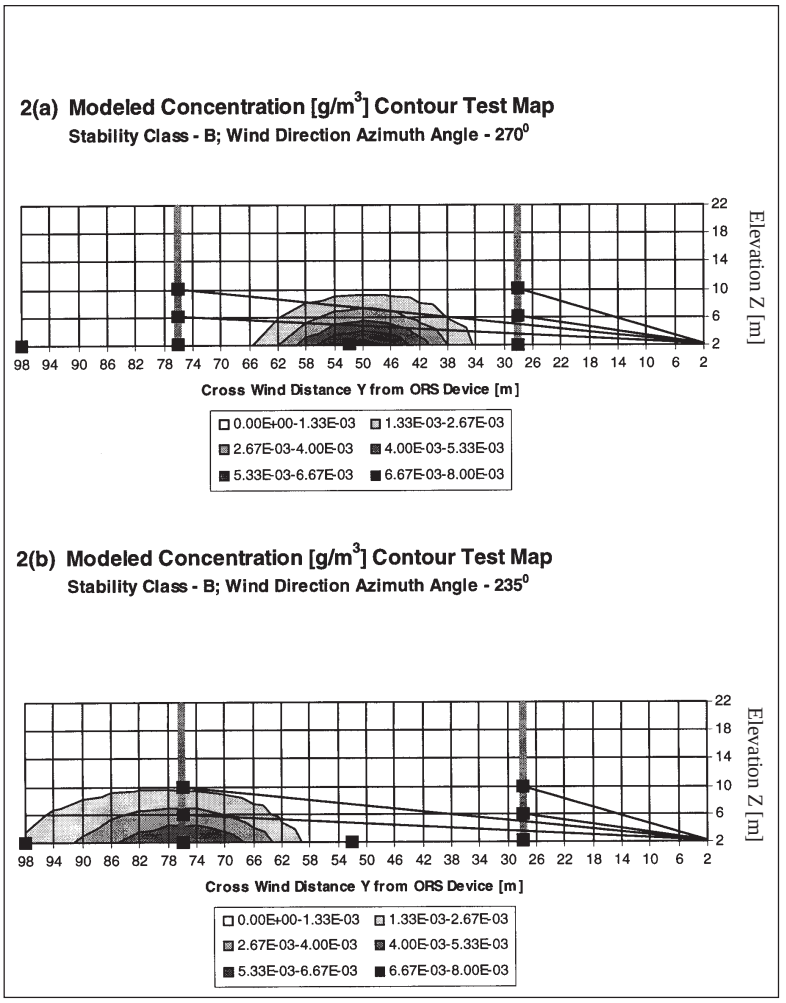

Figure 2. Examples of two modeled concentration contour maps calculated for the downwind vertical plane using the PAL dispersion model. The beam geometry is overlaid where the eight black squares show the retroreflectors: (a) wind direction azimuth angle of 270°; (b) wind direction azimuth angle of 235°.

Simulated PIC values were computed for each beam path for a given test map by integrating the projected length of the beam through each elementary square unit concentration and along the whole path length. Using relatively large elementary square units for the numerical integration procedure introduced some error into the simulated PIC values. Therefore, the calculated PIC values are not truly "noiseless." As described in the previous section, the authors applied SBFM-CT with the Simplex minimization algorithm to the simulated PIC values to solve for the bi-variate Gaussian unknown parameters. The authors assumed that the correlation factor is equal to 0 and did not apply any restrictions for the other five unknown parameters. As a first guess, the authors substituted the following values: $A=5$; $m_y=50$ m; $\sigma_y=10$ m; $m_z=2$ m; $\sigma_z=5$ m. The authors chose these values arbitrarily and applied them to all reconstructions executed in this study. Then, since the input wind speed was 1 m/sec, the reconstructed emission rate was calculated by numerical integration of the reconstructed bi-variate Gaussian followed by multiplication of the latter by the cosine of the wind shift angle.

First, the authors compared a beam geometry consisting of six paths scanning to one far tower, with a geometry of eight beam paths scanning to two towers, as illustrated in Figure 1. In the perpendicular situation, the reconstructed emission rate only reached the value of 0.9 (ideally it should be 1) for both beam geometries. This could be explained by the limited number of beams in all these configurations. The triangle data marks in Figure 3 show the change in reconstructed emission rate as a function of azimuth angle in wind direction for the eight-beam geometry. The six-beam geometry yielded the reasonably good reconstructed emission rate values compared to the eight-beam geometry, but only when the wind shifts were in the range of 215–290 (continuous line in Figure 3).

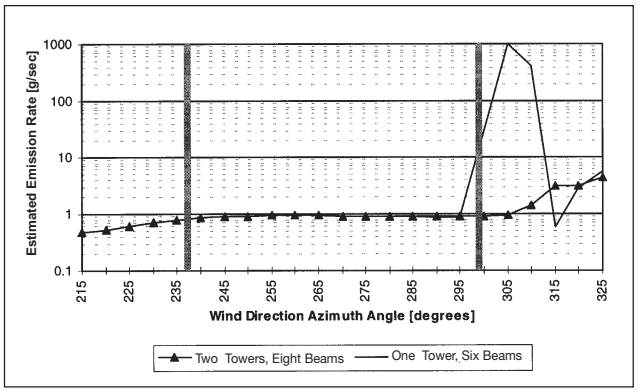

Figure 3. Estimated emission rate as a function of the wind direction azimuth angle for the six (one tower) and eight (two towers) beam geometries, calculated for stability class B and modeled emission rate of 1 g/sec. The location of towers projected in the angular domain is shown with the thick gray vertical lines (it is the angle created by a line connecting the point source and the tower and by the normal to the plane).

The authors also tried locating the PI-ORS device in the middle of the domain (at 52 meters in the positive *y* axis, see Figure 1) to retrieve a more symmetrical result for the reconstructed emission rate with regard to both directions of wind shifts. The PI-ORS device was simulated to scan in opposite directions over the same eight retroreflectors. This symmetric beam geometry was expected to yield symmetric response to shifts in wind directions; however, it severely underestimated the emission rate in the normal situation (0.55 compared to 0.9 in the previous beam geometry). Therefore, it appears from study results that the suggested beam geometry with two towers as in Figure 1 yielded the more robust estimates in the study.

Examination of the reconstructed parameters of the bi-variate Gaussian yielded an observation that there is some correlation between the deviation of the reconstructed parameters from the test map parameters and the estimated emission rate. For example, Figure 4 plots the difference between the test map cross-wind peak location and reconstructed cross-wind peak location as a function of the wind direction azimuth angle. As noted above in the emission rate study, good estimates of peak location are achieved when the peak falls between the two towers. Since the cross-wind peak location can be estimated by wind direction data when the source location is known, or can be estimated by applying a one-dimensional SBFM fitting procedure to the ground-level PIC data, this measure could provide an indication of a successful estimation of emission rate. The authors also found, in general, that the Simplex procedure tends to either totally fail (i.e., give nonlogical parameters) or to reasonably reconstruct the parameters followed by a reasonably good estimation of the emission rate.

As mentioned before, the authors examined different beam geometries for test maps generated for Pasquill stability class B with the PAL Gaussian dispersion model. As shown in Figure 2, this stability class produces relatively narrow plumes for a point source only 40 m upwind from the measurement beam geometry. From a previous field experiment in similar conditions, the authors learned that such narrow plumes are fairly uncommon. Much wider plumes should be considered for simulating 20-min average maps, especially when the release is not from a point source. As shown in Figure 5, running the same procedure for stability class A produced even more robust estimates of emission rates with regard to shifts in wind direction. We also tried to reconstruct Gaussian test maps with much smaller (σ_y=6 m and σ_z=2 m) and larger (σ_y=30 m and σ_z=10 m) standard deviations and retrieved very good reconstructions for both cases in the same beam geometry. These results indicate that the suggested methodology is not sensitive to plume width or stability class.

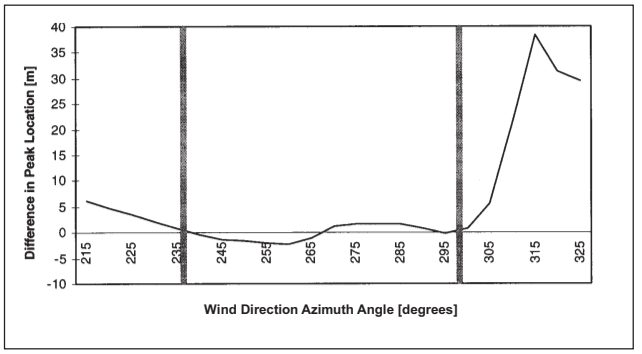

Figure 4. Difference between the test map cross-wind peak location and the reconstructed cross-wind peak location as a function of the wind direction azimuth angle. These values also can be interpreted as the percentage error in peak location compared to the total path length (which is 100 meters). The projected location of towers in the angular domain is shown with the thick gray vertical lines.

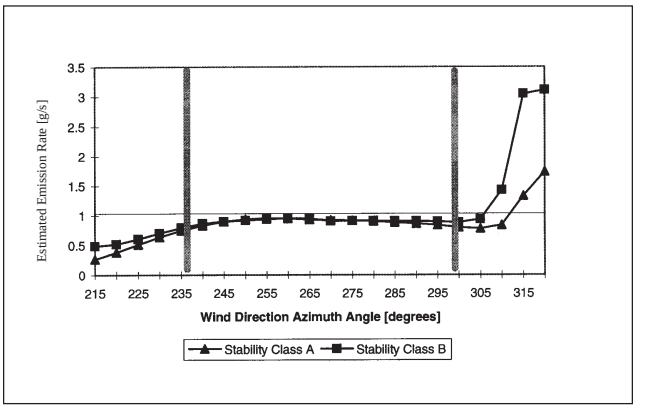

Figure 5. Estimated emission rate for stability classes B and A as a function of the wind direction azimuth. The projected location of towers in the angular domain are shown with the thick gray vertical lines. The horizontal line at 1 g/sec indicates the input modeled emission rate.

To simulate the fluctuation in PIC values as a function of the path length in the suggested beam geometry and scanning conditions, a field experiment was conducted. A bi-static BOMEM 155MB Open-Path FTIR beam path was located 40 meters downwind from the source and approximately perpendicular to the average wind direction. The general site configuration in the field experiment was described in a previous paper.[9] A 75-m OP-FTIR beam path was segmented into two shorter path lengths of 52 and 32 m. The OP-FTIR instrument continuously sampled spectra from each single scan of the interferometer for about two minutes on each beam segment. The spectral data (1 cm^{-1}) was converted to time-resolved PIC data of about two seconds for a data point, which the authors converted to 10-sec values by averaging five consecutive readings. As expected, the shortest path concentration data were drastically more variable, with more than 80% of the measured data under the instrument's detection limit. Although the average value of all scans was detectable, the standard deviation was more than twice the average, so the authors decided not to rely on the PIC data from the shortest path. Based on results from the longer paths, the authors found that variability in the concentration data could be described by the following equation:

$$\frac{\sigma_x}{\bar{x}} = A \cdot L^{-\alpha} \qquad (3)$$

where $\frac{\sigma_x}{\bar{x}}$ is the coefficient of variation (standard deviation over the average), L is the path length, and A and α are parameters to fit to the measured data. Based on the data acquired in the field experiment, the authors found that $A \sim 4800$ and $\alpha \sim 2.34$. The authors assigned a different error term, according to eq 3, to each of the simulated PIC values integrated from the test maps using a computerized random number generator that produces normally distributed random numbers. The random number was then normalized to PIC values considering the relevant path length. For each beam path, the authors repeated this error term an additional 10 times to simulate the measurement errors in the PIC values in the suggested scanning procedure. Then the authors averaged the different values to retrieve the equivalent value for a PIC over a 20-min period and performed the methodology procedure on the simulated "noisy" averaged PIC values to retrieve an estimate of the emission rate. For each wind direction, the authors repeated this procedure 300 times wherein each time a different set of averaged PIC values was applied. An average and standard deviation of the 300 values of estimated emission rate were calculated for each of the wind directions.

Figure 6 shows the results of the study simulating measurement errors. Between the two towers, the average of the "noisy" emission rate values nicely follows the "noiseless" emission rate values calculated before and shown in Figure 3. As expected, the standard deviations are inflated gradually as the wind rotates toward the ORS device. However, on the other end, the standard deviations grow smaller as the wind rotates away from the ORS instrument even beyond the far end tower.

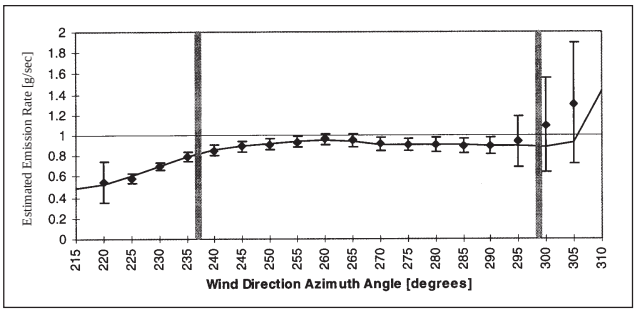

Figure 6. Averaged estimated emission rate from the SBFM-CT reconstructions (diamond marks) and standard deviations (error bars $\pm$ SD) in 300 runs of PIC data with simulated random noise as a function of the wind direction azimuth angle. The solid line through the data points represents the estimated emission rate from PIC data without simulated random noise, in the same stability class (class B). The projected tower locations in the angular domain are shown with the thick gray vertical lines. The horizontal line at 1 g/sec indicates the input modeled emission rate.

CONCLUSIONS

The authors found the CT SBFM approach for estimating the emission rate to be very robust to atmospheric conditions, realistic simulations of measurement errors, and source configuration as long as the average wind direction vector intersecting the emission source is pointing between the two towers. If a wider range of wind direction is desired, one can move the towers away from each other and move back the PI-ORS device to compensate.

In some cases, like this study, the simpler local search, like the Simplex algorithm, was found to be sufficient. First, applying a one-dimensional SBFM approach to the ground-level segmented beam paths would allow us to provide a very close first guess for the solution. As σ_z is strongly correlated to σ_y for a given atmospheric stability, source configuration, and downwind distance from the source, a reasonably good first guess can be estimated for σ_z as well. One also could substitute values from the one-dimensional SBFM reconstruction along the ground level as fixed parameters for m_y and σ_y of the bi-variate Gaussian to afford more degrees of freedom in the two-dimensional SBFM solution for A, m_z, and σ_z.

In the future, an experimental validation of a PI-ORS monitoring system for estimating emission rates is expected. This technology should provide fairly robust estimates of the total emission from many kinds of fugitive

sources along with the selection of an adequate PI-ORS device. Based on the experimental data of the validation study, the authors will explore ways for such a monitoring system to provide estimates with better time resolution than the simulated 20 min.

Such a system could be applied in a continuous monitoring mode to function also as an alarm for departure from normal working conditions of many kinds of area and volume emission sources. In this case the system's beam geometry should be located between the emission source and the concerned neighboring communities or workers' location to alert them to a potential emergency. Reconstructed maps should be able to provide measures of the initial near field dispersion parameters. These parameters as atmospheric stability condition indicators, along with the estimated flux, could be input into a dispersion model to calculate in near real time the downwind field of concentrations.

ACKNOWLEDGMENTS

This research was partially supported by the Consortium for Risk Evaluation with Stakeholder Participation through Department of Energy (DOE) Cooperative Agreement #DE-FC01-95EW55084. This support does not constitute an endorsement by DOE of the views expressed in this article. This research was partially supported by the National Institute for Occupational and Safety Health Grant # RO1OH02660.

REFERENCES

1. Scotto, R.L.; Minnich, T.R.; Leo, M.R. A Method for Estimating VOC Emission Rates from Area Sources Using Remote Optical Sensing. In *Proceedings of the EPA/AWMA International Symposium on the Measurement of Toxic and Related Air Pollution*, Raleigh, NC, 1991; 698.
2. Minnich, T.R.; Scotto, R.L.; Leo, M.R.; Sanders, B.C.; Perry, S.H.; Pritchett, T.H. A Practical Methodology Using Open-Path FTIR Spectroscopy to Generate Gaseous Fugitive-Source Emission Factors at Industrial Facilities. In *Proceedings of the SP-81 Optical Remote Sensing, Application to Environmental and Industrial Safety Problems, Houston, TX*, Pittsburgh, PA, 1992; 513.
3. Milton, M.J.T.; Partridge, R.H.; Goody, B.A. Minimum Emission Rates Detectable from Landfill Sites Using Optical Integrated-Path Techniques. In *Proceedings of the A&WMA International Specialty Conference on Optical Sensing for Environmental and Process Monitoring, VIP-55 San Francisco 1995*, Pittsburgh, PA, 1996; 393.
4. Piccot, S.D.; Masemore, S.S.; Lewis-Bevan, W.; Ringler, E.S.; Harris, D.B. "Field assessment of a new method for estimating emission rates from volume sources using open-path FTIR," *J. Air & Waste Manage. Assoc.* **1996**, *46*, 159.
5. Piccot, S.D.; Masemore, S.S.; Ringler, E.S.; Srinivasan, S.; Kirchgessner, D.A.; Herget, W.F. "Validation of a method for estimating pollution emission rates from area sources using open-path FTIR spectroscopy and dispersion modeling techniques" *J. Air & Waste Manage. Assoc.* **1994**, *44*, 271.
6. Kirchgessner, D.A.; Piccot, S.D.; Chadha, A. "Estimation of methane emissions from a surface coal mine using open path FTIR spectroscopy and modeling techniques," *Chemosphere* **1993**, *26(1–4)*, 23.
7. Simpson, O.A.; Kagan, R.H. Measurements of Emissions at a Chemical Waste Water Site with an Open Path Remote Fourier Transform Interferometer. In *Proceedings of the EPA/A&WMA International Symposium on the Measurement of Toxic and Related Air Pollution*, Raleigh, NC, 1990; 937.
8. Whitcraft, W.K.; Wood, K.N. Use of Remote Sensing to Measure Wastewater Treatment Plant Emissions. In *Proceedings of the 83rd Annual Meeting & Exhibition of the A&WMA*, Pittsburgh, PA, 1990.
9. Hashmonay, R.A.; Yost, M.G.; Mamane, Y.; Benayahu, Y. "Emission rate apportionment from fugitive sources using open-path FTIR and mathematical inversion," *Atmos. Environ.* **1999**, *33(5)*, 735-743.
10. Walmsley, H.L.; O'Connor, S.J. The Use of Differential Absorption LIDAR to Measure Atmospheric Emission Rates at Industrial Facilities. In *Proceedings of the A&WMA International Conference on Optical Sensing for Environmental and Process Monitoring, Dallas, Texas, November 1996*, Pittsburgh, PA, 1997; 127.
11. Hashmonay, R.A.; Yost, M.G.; Wu, C.F. "Computed tomography of air pollutants using radial scanning path-integrated optical remote sensing," *Atmos. Environ.* **1999**, *33(2)*, 267-274.
12. Price, P.N. "Pollutant tomography using integrated concentration data from non-intersecting optical paths," *Atmos. Environ.* **1999**, *33(2)*, 275-280.
13. Drescher, A.C.; Gadgil, A.J.; Price, P.N.; Nazaroff, W.W. "Novel approach for tomographic reconstruction of gas concentration distributions in air: use of smooth basis functions and simulated annealing," *Atmos. Environ.* **1996**, *30(6)*, 929.
14. Drescher, A.C.; Park, D. Y.; Yost, M.G.; Gadgil, A.J.; Levine, S.P.; Nazaroff, W.W. "Stationary and time-dependent indoor tracer-gas concentration profiles measured by OP-FTIR remote sensing and SBFM Computed Tomography," *Atmos. Environ.* **1997**, *31(5)*, 727.
15. Press, W.H.; Teukolsky, S.A.; Vetterling, W.T.; Flannery, B.P. *Numerical Recipes in FORTRAN*, 2nd ed.; Cambridge University Press: Cambridge, MA, 1992.
16. Petersen, W.B.; Rumsey, E.D. *User's Guide for PAL 2.0, A Gaussian-Plume Algorithm for Point, Area, and Line Sources;* EPA/600/8-87/009; NTIS PB87-168787; U.S. Environmental Protection Agency: Research Triangle Park, NC, 1987.
17. Hanna, S.R.; Briggs, G.A.; Hosker, Jr., R.P. *Gaussian Plume Model for Continuous Sources, Handbook on Atmospheric Diffusion*; Technical Information Center, U.S. Department of Energy, 1982; 25–35.

About the Authors

Dr. Ram A. Hashmonay, M.S., Sc.D., is a research associate at the University of Washington, Department of Environmental Health, Box 357234, Seattle, WA 98195. Dr. Michael G. Yost, M.S., Ph.D., is an associate professor and director of the Industrial Hygiene program at the University of Washington, Department of Environmental Health, Box 357234, Seattle, WA 98195.